ACS Energy LETTERS

Cite This: ACS Energy Lett. 2019, 4, 1521−1527

http://pubs.acs.org/journal/aelccp

LETTER

Suppressed Ion Migration in Reduced-Dimensional Perovskites Improves Operating Stability

Ziru Huang,[†] Andrew H. Proppe,[†,‡] Hairen Tan,[†,§] Makhsud I. Saidaminov,[†] Furui Tan,[†,∥] Anyi Mei,[†,⊥] Chih-Shan Tan,[†] Mingyang Wei,[†] Yi Hou,[†] Hongwei Han,[⊥] Shana O. Kelley,[‡,#] and Edward H. Sargent*[,†]

[†]Department of Electrical and Computer Engineering, University of Toronto, 35 St. George Street, Toronto, Ontario M5S 1A4, Canada

[‡]Department of Chemistry, University of Toronto, 80 St. George Street, Toronto, Ontario M5S 3G4, Canada

[§]National Laboratory of Solid State Microstructures, Collaborative Innovation Centre of Advanced Microstructures, Jiangsu Key Laboratory of Artificial Functional Materials, College of Engineering and Applied Sciences, Nanjing University, Nanjing, Jiangsu 210093, China

[∥]Key Lab of Photovoltaic Materials, Department of Physics and Electronics, Henan University, Kaifeng 475004, China

[⊥]Michael Grätzel Center for Mesoscopic Solar Cells, Wuhan National Laboratory for Optoelectronics, Huazhong University of Science and Technology, Wuhan, Hubei 430074, China

[#]Department of Pharmaceutical Sciences, Leslie Dan Faculty of Pharmacy, University of Toronto, Toronto, Ontario M5S 3M2, Canada

Supporting Information

ABSTRACT: **Impressive progress in halide perovskite solar cells motivates further work to improve operating stability. It is known that ion-migration-driven decomposition represents a degradation pathway in perovskite solar cells and that it can occur within the perovskite material even in well-encapsulated devices. Here we find that quasi-two-dimensional (2.5D) perovskites suppress this ion-migration-induced degradation. Using TOF-SIMS, we confirm that iodide migration occurs in bulk perovskite photovoltaic devices operating at their maximum power point (MPP). We observe that iodine ions migrate across the spiro-OMeTAD layer to the spiro/gold contact interface, oxidizing and deteriorating the gold at the interface. In contrast, we find that large ⟨*n*⟩ 2.5D perovskites exhibit a significantly reduced rate of ion migration compared to 3D devices and exhibit less than 1% relative PCE loss in over 80 h of continuous operation at MPP, whereas the PCE of 3D devices diminishes by more than 50% within the first 24 h.**

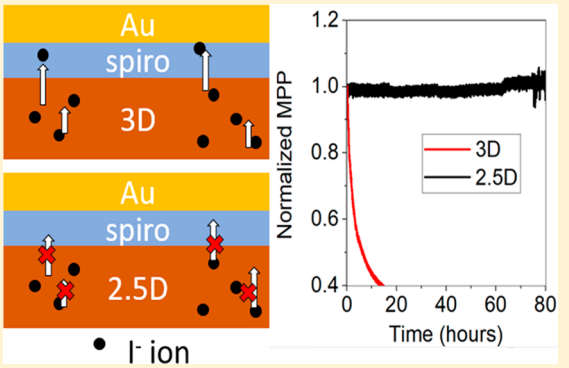

Today's perovskite solar cells (PSCs) require additional effort on stability, especially under maximum power point (MPP) operating conditions.[1−5] Perovskites have two main decomposition pathways at room temperature: one arises due to moisture and oxygen-induced hydration and oxidization of the perovskite and another is ion-migration-driven decomposition.[6−11] The first process can be addressed by encapsulants such as those employed in commercial solar cell modules.[12−15]

The second process, ion migration, is associated with the low formation energy of the perovskite lattice and involves the movement of ions especially under solar cell working conditions. This can occur even in encapsulated devices. It leads to the formation of vacancies or undesirable complexes.[10,16−19] It has been shown that ion migration can cause the formation of PbI_2 belts in $MAPbI_3$ under a high applied bias, which is believed detrimental to long-term performance.[10] This behavior needs to be addressed through improvements to the perovskite active layer itself.

Recently, PSCs with active layers composed of mixed-dimensional perovskites (also known as Ruddlesden−Popper or quasi-two-dimensional (2.5D) perovskites) have shown

Received: April 25, 2019
Accepted: May 31, 2019

DOI: 10.1021/acsenergylett.9b00892
ACS Energy Lett. 2019, 4, 1521−1527

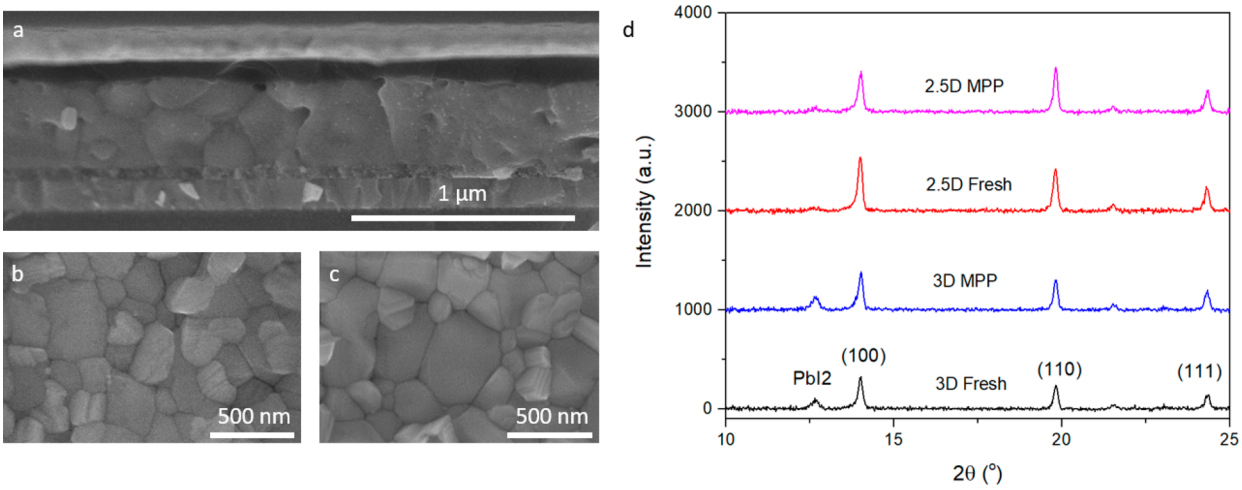

Figure 1. Morphological and crystallographic properties of the 3D and 2.5D perovskites studied in this work. (a) Cross-sectional SEM image of a full PSC. Top-view SEM images of (b) 3D and (c) 2.5D perovskite films. (d) XRD data for 3D and 2.5D full PSCs under different aging conditions.

indications of promising stability compared to analogous 3D PSCs.[20−26] Lower-dimensional perovskites are formed through the addition of bulky ammonium cation ligands (typically phenethylammonium, PEA, or butylammonium, BTA), which can substitute A-site cations (e.g., methylammonium, formadinium, or cesium) (FA = $HC(NH_2)_2^+$, MA = $CH_3NH_3^+$) and form a layer of protective hydrophobic organic molecules that terminate the perovskite lattice. Hydrophobic terminating organic layers help prevent water from penetrating into the material.[20,21,27] Density functional theory (DFT) calculations have shown that the removal of these bulky cations from the lattice requires significantly higher energies than does the removal of smaller A-site cations like MA or FA, indicating another basis of improved stability.[27]

The relationship between perovskite dimensionality and ion migration remains underexplored. Temperature-dependent conductivity studies have revealed that the activation energy for ion migration in low-n 2.5D perovskites ($\langle n \rangle = 3$) exceeds that in bulk perovskites.[28] These studies focused on the active material itself rather than full devices, and the identity of migrating species was not reported. Additionally, solar cells with active layers composed of strongly confined, low-dimensional 2.5D perovskites (typically $n \leq 5$) typically exhibit low PCEs and are therefore not suitable for applications in highly efficient photovoltaics.[20,27] Studies of 2D/3D perovskite heterostructures have shown improved long-term stability but do not directly address the challenge of ion migration within the 3D layer and have been seen to suffer an initial loss of PCE (termed a fast burn-in).[29] Ion migration in 2.5D perovskites with higher average quantum well widths ($n \geq 20$) has not been thoroughly examined nor has the relationship between 2.5D perovskites and device operating (AM1.5 at MPP) stability, as distinct from ambient stability (shelf life).

Here we study vertical ion migration and investigate how this affects performance degradation in planar n−i−p PSCs under ambient working conditions, comparing the use of 2.5D vs 3D active layers. We find that 2.5D perovskites ($n = 40$) that employ the ligand allylammonium (ALA) provide improved operating stability compared to their 3D counterparts. With the aid of time-of-flight secondary ion mass spectroscopy (TOF-SIMS), we report that the main species undergoing vertical ion migration is iodine. We observe that iodine migrates through the organic hole transport layer (HTL) to the metal contact atop the device, deteriorating the HTL and HTL/metal interface. Comparing the TOF-SIMS profiles of 2.5D and 3D perovskites in the same device architectures and aging conditions, we find 75% less Au_2I signal at the HTL/metal interface and 60% lower change in iodine signal in the HTL for the 2.5D device, indicating that 2.5D perovskites exhibit significantly slower vertical iodine migration in planar n−i−p devices. We further analyze the impact of ion migration on device stability, finding that iodide migration is deleterious to MPP stability and that the suppressed migration in 2.5D devices helps MPP stability under inert conditions. With this suppressed ion migration, we achieved a 19.9% PCE 2.5D photovoltaic device with no observable PCE decrease after operating under MPP tracking conditions for 80 h, whereas the 3D device degraded by more than 50% following the first 24 h of MPP operation.

To study the impact of ion migration on the long-term operation of PSCs, we fabricated control devices using the planar n−i−p structure ITO/TiO_2/perovskite/spiro-OMeTAD/Au. The perovskite layer has a triple cation/anion composition of $Cs_{0.05}FA_{0.8}MA_{0.15}PbI_{2.88}Br_{0.04}Cl_{0.08}$. To synthesize the 2.5D perovskite active layers, we substituted 5% (molar ratio) of the A-site cations with the organic ligand molecule ALA in the precursor solution. This corresponds to an average of $n = 40$ layers per grain (n = number of monolayers in perovskite). We selected ALA as the ligand because, compared to other bulky organic ligand molecules such as PEA and BTA, ALA provides a smaller population of lower-n perovskite quantum wells.[30] This provides a smoother energy landscape within the film and at the same time offers similar dark stability to that provided by PEA and BTA.[27,30] The device structure is shown in Figure 1a.

We first looked for morphological differences correlated with ALA incorporation. In Figure 1b,c, we show scanning electron microscope (SEM) images of the 3D and 2.5D perovskite films. The pristine 3D perovskite film shows a pinhole-free surface, which indicates no shunt in the perovskite layer. The 2.5D perovskite is similar to the 3D perovskite film, with some flake-like stacking structures corresponding to the 2.5D perovskite.[21]

DOI: 10.1021/acsenergylett.9b00892
ACS Energy Lett. 2019, 4, 1521−1527

To provide an initial stability comparison between 3D and 2.5D perovskite, we aged the devices under a N_2 atmosphere at room temperature to exclude oxygen. This also allowed us to exclude moisture and heat-induced degradation of the perovskites. We then compared X-ray diffraction (XRD) patterns before and after aging (Figure 1d). Even in inert conditions, the 3D devices show a significant increase in PbI_2 after aging. For 3D perovskites, the PbI_2/perovskite XRD peak ratio increased over 20% after aging compared to fresh 3D samples, whereas for 2.5D perovskite, the PbI_2/perovskite ratio stayed the same (Table 1). We note that the PbI_2 peak in XRD is very sensitive to the film composition, and even a few percent excess of PbI_2 can give rise to a large PbI_2 signal in XRD.[30,31] This sensitivity enables us to report a signal related to the degradation of perovskite in a N_2 atmosphere, but we point out that the peak area represents a *relative* change in the amount of PbI_2 before vs after aging.

Table 1. Comparison of the Change of Ratio of PbI_2 and Perovskite for 3D and 2.5D PSCs after Aging at MPP in N_2

	perovskite peak area (counts × degree)	PbI_2 peak area (counts × degree)	PbI_2/perovskite peak area ratio
3D fresh	47	16	0.33
3D MPP 60 h	56	22	0.40
2D fresh	80	10	0.13
2D MPP 60 h	62	9	0.14

We also looked for changes in carrier dynamics related to the incorporation of ALA. Figure 2a,b shows the steady-state photoluminescence (PL) and time-resolved photoluminescence (TRPL) of the 3D and 2.5D perovskites. The samples are encapsulated using poly(methyl methacrylate) (PMMA) to avoid degradation from oxygen and moisture.[31,32] We observe that the PL peak position shows no notable difference between 2.5D and 3D perovskites, a result of the high $\langle n \rangle$ value in the 2.5D case: the quantum confinement of the $n = 40$ grains is too small to be spectrally resolved, in agreement with previous observations.[33] Figure 2c shows the change of PL intensity versus time for the 3D and 2.5D perovskite films. The PL intensity of 3D perovskite quickly decreases while the 2.5D perovskite remains stable: for the 2.5D perovskite, its change compared to its initial value is less than 20% relative as a result of 10 h of aging under photoexcitation.[34]

To characterize any ion migration and to determine the identity of moving species in working devices, we carried out TOF-SIMS measurements on fresh vs MPP-operated devices. We operated both the 3D and 2.5D perovskite devices under AM1.5 conditions at MPP in nitrogen at room temperature. We first measured the depth profile of fresh and aged 3D and 2.5D devices (Figures S1 and S2) and compared all major ion species. As the I^- and FA^+ counts in the perovskite layer saturated the detector, we also provide depth-dependent traces for I_2^- and ^{13}C-FA in Figures S1, S2, and S4. The Pb, FA, MA, and Cs ions show no major difference (Figures S3–S6) before and after aging for both 3D and 2.5D perovskites. However, in the 3D perovskite, the iodine signal shows prominent changes, especially at the interface between the gold and spiro-OMeTAD (hereafter referred to just as spiro) layers (Figure S2), while the 2.5D device shows little change (Figure S1).

We conclude that I^- is the dominant species migrating during these experiments and that the $n = 40$ 2.5D perovskite suppresses this migration (Figure 3a). Figure S7 shows the 3D tomography reconstruction from the TOF-SIMS experiments, and it indicates the uniformity and low concentration of I^- in the spiro layer in the fresh device. We conclude that in the present study the I^- signal away from the perovskite layer is a result of migration and not due to permeation of ions through large pinholes.[35]

We also identified a significant amount of Au_2I^- signal in the TOF-SIMS spectra. We note that this signal does not directly confirm the existence of such a complex at the interface; it is possible that this complex forms following the sputtering pulse in our TOF-SIMS experiments before being swept into the detector (i.e., the sputtering of two gold atoms and one iodine atom leads to the formation of a singly charged secondary ion complex shortly upon entering the vacuum after being sputtered from the sample). It does, however, confirm the presence of iodine at this interface. The depth profile shows that the Au_2I^- signal has increased significantly in aged 3D perovskite devices compared to fresh devices (Figure 3b). In contrast, in the case of the 2.5D perovskite, the Au_2I^- signal is unchanged before and after aging (Figure 3c).

These findings suggest that in 3D devices, I^- migrates from the perovskite layer through the spiro layer and all the way to the spiro/gold interface in MPP operating devices even at room temperature in a nitrogen atmosphere. In $n = 40$ 2.5D perovskite devices, this migration is greatly suppressed: comparing the ratio of Au_2I^- signal at the gold/spiro interface before and after aging, we see that this signal increases roughly

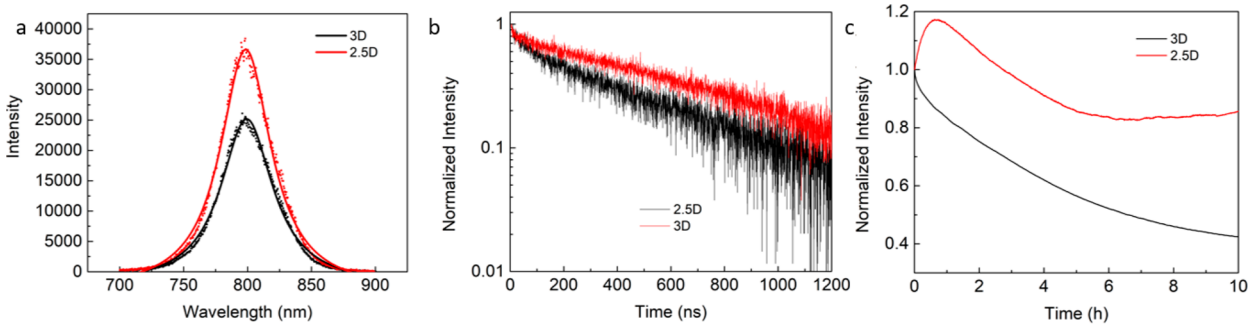

Figure 2. PL investigations of 3D and 2.5D perovskites, including when aged under pulsed photoexcitation. (a) Steady-state PL spectra of 3D and 2.5D perovskites. (b) TRPL decay of 3D and 2.5D perovskites. (c) Normalized PL peak intensity over time under pulsed laser illumination.

DOI: 10.1021/acsenergylett.9b00892
ACS Energy Lett. 2019, 4, 1521−1527

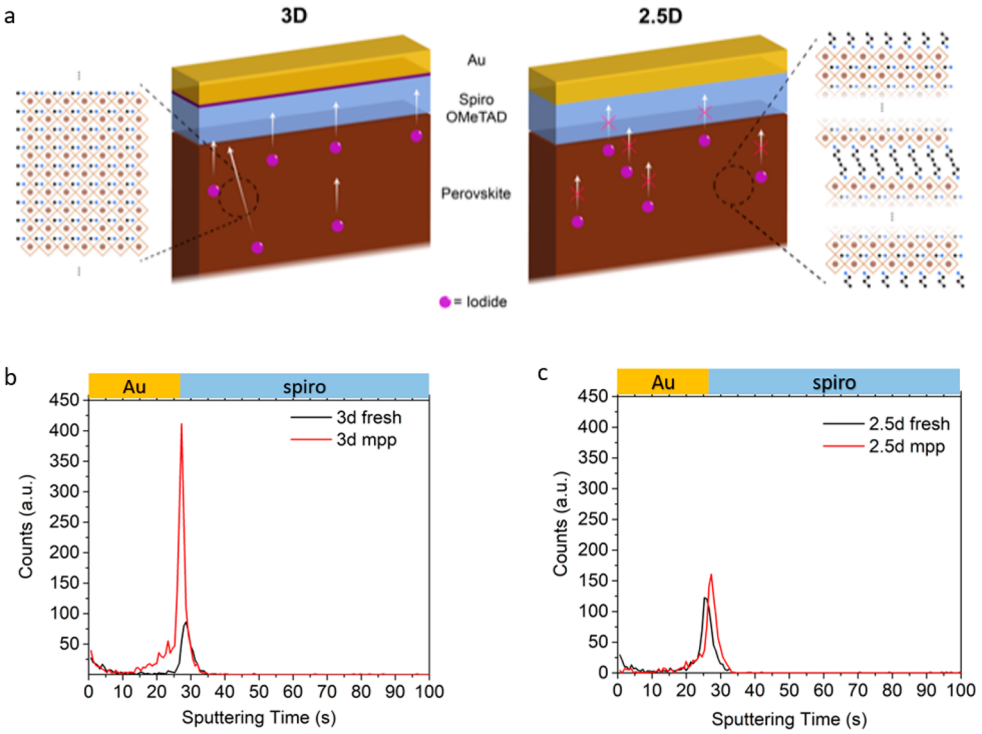

Figure 3. TOF-SIMS investigations of ion migration in 3D and 2.5D devices following operation at MPP for 60 h. (a) Schematic of iodine ion migration throughout the entire 3D perovskite device and suppressed migration in the 2.5D perovskite device. (b) Comparison of the Au_2I^- depth profile of a fresh 3D perovskite and an aged 3D perovskite device. (c) Comparison of the Au_2I^- depth profile of a fresh 2.5D perovskite and an aged 2.5D perovskite device.

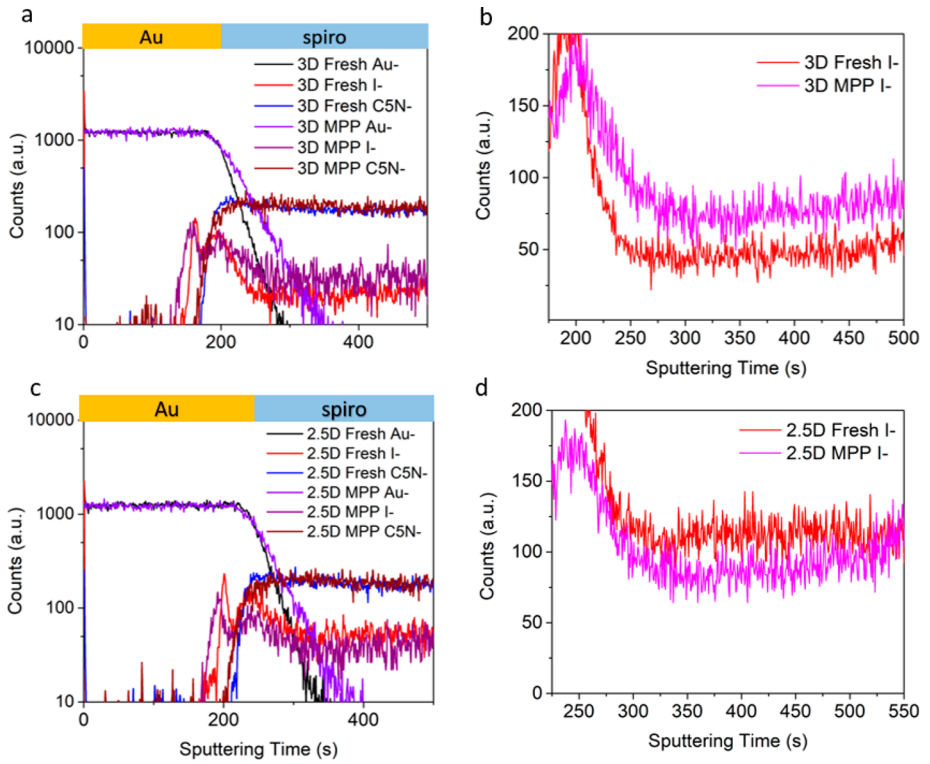

Figure 4. Slower TOF-SIMS operation directly proves the iodine migration in the 3D device and its suppression in the 2.5D device. Scans here were performed with a slower sputtering rate to target the Au and spiro layers of the device. (a) TOF-SIMS depth profile of a fresh and aged 3D PSC and (b) comparison of iodine signal in the spiro layer. (c) TOF-SIMS depth profile of a fresh and aged 2.5D PSC and (d) comparison of iodine signal in the spiro layer in slower scans.

DOI: 10.1021/acsenergylett.9b00892
ACS Energy Lett. 2019, 4, 1521−1527

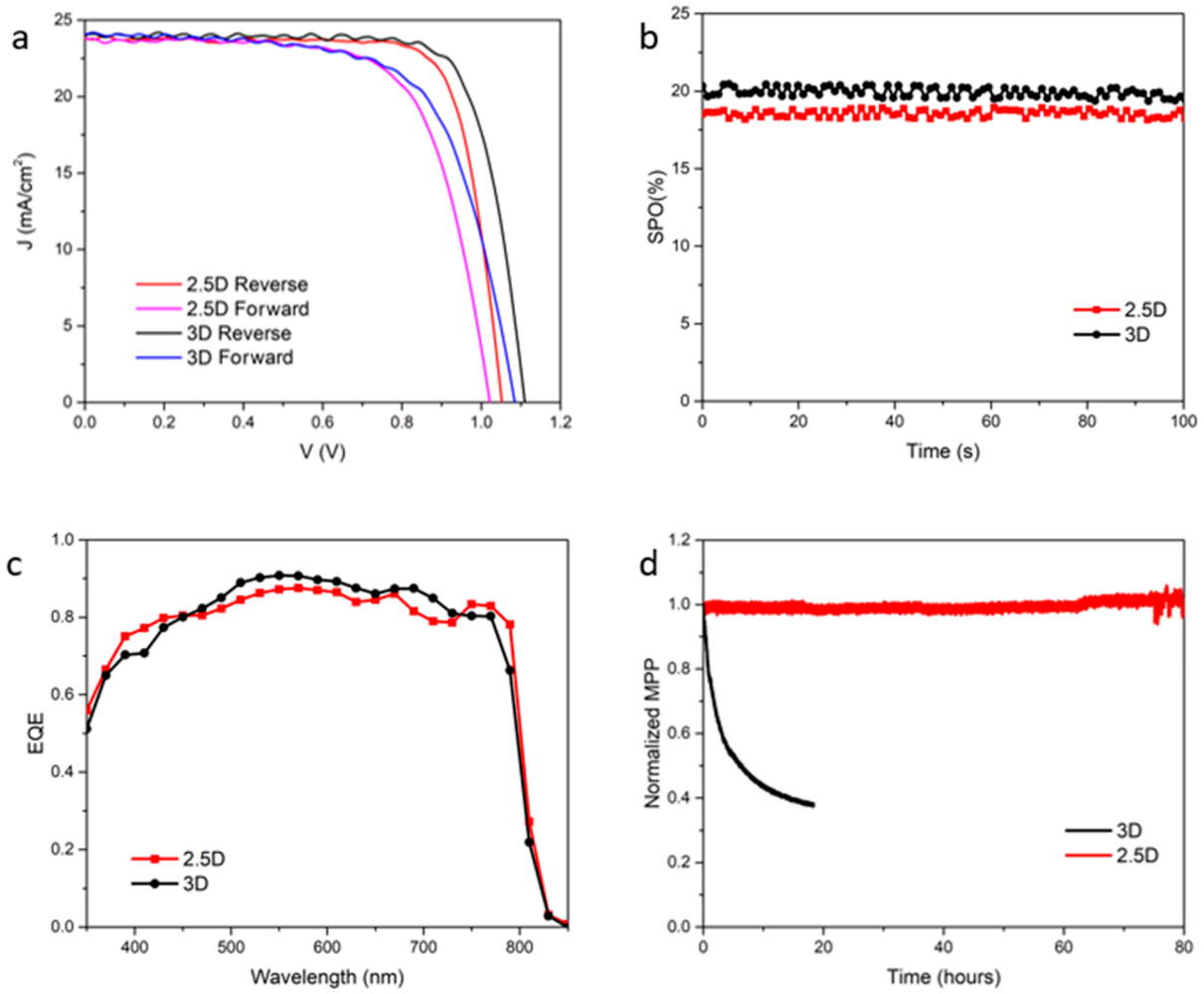

Figure 5. Device performance and stability. (a) *J*–*V* curves of 3D and 2.5D PSCs (data have been smoothed using a moving average filter). (b) Stabilized power output of the champion 3D and 2.5D devices. (c) EQE of the champion 3D and 2.5D devices. (d) Evolution of efficiency of 3D and 2.5D devices at MPP. Values are normalized to the initial PCE at MPP.

×5 for the 3D devices, whereas the increase is only about ×1.25 for the 2.5D devices.

We performed additional TOF-SIMS experiments with slower sputtering rates in order better to resolve ion migration within the Au and spiro layers of the device. Plots of Au^-, I^-, and C_5N^- versus sputtering depth are shown in Figure 4 for the 3D (Figure 4a) and 2.5D (Figure 4c) devices. Because these devices are aged at room temperature, Au does not penetrate through the spiro layer but exists only in the surface layer.[36] Figure 4b,d presents enlarged figures that show the I^- distribution in the spiro layer for fresh and MPP aged 3D and 2.5D devices, respectively. The MPP-operated 3D perovskite device exhibits a 60% higher I^- signal than fresh devices throughout the spiro layer, while the 2.5D perovskite shows a much smaller change following the same duration of AM1.5 MPP operation. This directly proves the iodine migration throughout the spiro and gold layers in the 3D device and the suppression of iodine migration in the 2.5D perovskite device.

To investigate further iodine migration in 3D perovskites, we carried out sputtering X-ray photoelectron spectroscopy (XPS) of full devices, sputtering from the top of the gold layer through to the gold/spiro interface and further into the spiro layer, keeping track of the elements Au, I, and N at the various sputter depths (Figure S8). We observed that the Au counts decrease significantly at line scan 5, corresponding to the Au/spiro interface. Upon reaching this interface, in the aged sample, a shoulder peak with higher binding energy appears in the Au 4f spectrum: the binding energy of Au $4f_{7/2}$ for Au^0 is ~84.2 eV, whereas oxidized gold Au^+ has a binding energy of ~85.6 eV.[37] These values are consistent with the peak positions we see in our Au 4f spectra, indicating oxidation of Au near the spiro/gold interface. No such peak is observed in fresh samples. This suggests that gold forms complexes with iodine that have migrated to this interface as this is observed to be the dominant species migrating during device operation. We note that these oxidized peaks do not appear as a result of damage to the material during the sputtering process because mostly Au^0 peaks are again obtained after sputtering deeper into the material, and no extra peaks are observed in the fresh samples that are sputtered under identical conditions.

From these experiments, we conclude that iodide ions are activated within the perovskite active layer under MPP conditions and that they migrate within the active layer but also through the spiro layer before they reach the spiro/gold interface. This study identifies that at room temperature the moving species are indeed I^- ions rather than metal ions.[36,38] This migration and the subsequent deterioration of the Au/spiro interface is much more severe in the 3D device compared

DOI: 10.1021/acsenergylett.9b00892
ACS Energy Lett. 2019, 4, 1521−1527

to that in the 2.5D device, and this agrees with the ability of 2.5D perovskites to suppress iodide ion migration in MPP conditions.

To examine the influence of this ion migration on photovoltaic performance, we studied the MPP stability of PSCs based on 3D and 2.5D devices. The current−voltage (J−V) characteristics of champion devices are given in Figure 5a, and the performance metrics are summarized in Table 2. The

Table 2. Photovoltaic Parameters of the 2.5D and 3D PSCs

	V_{oc} (V)	J_{sc} (mA/cm^2)	PCE (%)	FF (%)
2.5D reverse	1.05	23.9	19.9	79
2.5D forward	1.02	23.8	16.8	69
3D reverse	1.11	23.6	20.8	79
3D forward	1.09	23.7	17.6	68

external quantum efficiency (EQE) is shown in Figure 5c. The stable output at MPP gives 20% PCE for the 3D device and 19% for the 2.5D device (Figure 5b), demonstrating that high average n value 2.5D perovskites provide a similar performance to 3D devices.[27] When the devices are operated at MPP in a nitrogen atmosphere, the 3D devices degrade rapidly, losing more than 50% of their initial PCE within 24 h of operation. In contrast, the 2.5D device shows no change in performance following 80 h of continuous AM1.5 MPP operation (Figure 5d). In contrast with other reports of MPP stability for 2.5D perovskites, we do not observe an initial burn-in.[21,22]

Because the MPP tests are performed at room temperature under a nitrogen atmosphere, oxygen- and water-induced degradation pathways can be ruled out. We conclude that the main degradation of these devices comes from ion migration, consistent with the observed iodide migration in 3D perovskite devices and suppressed migration in 2.5D perovskite devices.

To further evaluate how the ALA molecules suppress ion migration and stabilize the perovskite, we also tested the stability of ALA-post-treated devices under the same operating conditions. We found that post-treated devices do not show an appreciable difference in stability compared to the pure 3D device (Figure S9). Covering the surface of the perovskite with ligands is thus not sufficient to suppress ion migration: we offer that the formation of 2.5D structured grains, with their more negative (more favorable) formation energy, is key to stabilization.

To conclude, this work investigated degradation processes within n−i−p planar PSCs in inert photovoltaic working conditions. By comparing fresh and MPP aged devices operating in an inert atmosphere, we correlate vertical ion migration in a planar n−i−p device with degradation of operating performance. The studies are designed such that they exclude external factors such as oxygen and moisture. We also identified iodide ions to be the dominant migrating species. We are the first to report that iodide ions are sufficiently activated under standard working conditions to migrate within the perovskite active layer, penetrate through the spiro layer, and reach the spiro/Au interface, where they possibly form an iodine−gold complex. We saw that forming 2.5D perovskites by adding ALA ligands suppresses this migration and allows for significantly enhanced stability. The 2.5D PSC has an initial PCE of 19.9% that shows no degradation (including no initial drop in efficiency due to burn-in) following 80 h of continuous AM1.5 operation at MPP, whereas PSCs with 3D active layers show an initial PCE of 20% that degrades to an AM1.5 PCE of less than 10% within 24 h of operation. This work offers insights into the degradation mechanisms in PSCs in inert MPP conditions and highlights how 2.5D perovskites can contribute to increased stability in PSCs, in addition to their effects of protecting against moisture- and oxygen-induced degradation. To retard further the migration of other atoms, other layers can be modified. For example, gold migration can occur at 70 °C, and adding Cr can suppress this process.[36] Such modifications, along with the use of 2.5D perovskites, can be expected to improve stability further.

■ ASSOCIATED CONTENT

Supporting Information

The Supporting Information is available free of charge on the ACS Publications website at DOI: 10.1021/acsenergylett.9b00892.

Materials and Methods, Figures S1−S9 showing TOF-SIMS profiles and mapping, sputtering XPS, and normalized PCS versus time plots (PDF)

■ AUTHOR INFORMATION

Corresponding Author

*E-mail: ted.sargent@utoronto.ca.

ORCID

Ziru Huang: 0000-0001-7983-913X
Yi Hou: 0000-0002-1532-816X
Hongwei Han: 0000-0002-5259-7027
Shana O. Kelley: 0000-0003-3360-5359
Edward H. Sargent: 0000-0003-0396-6495

Notes

The authors declare no competing financial interest.

■ ACKNOWLEDGMENTS

This publication is based on work supported by the U.S. Department of the Navy, Office of Naval Research (Grant Award No.: N00014-17-1-2524). M.I.S. acknowledges the support of the Banting Postdoctoral Fellowship Program, administered by the Government of Canada. A.H.P. acknowledges support from the NSERC Alexander Graham Bell Scholarship program. The authors thank Dr. P. M. Brodersen in the Ontario Centre for Characterization of Advanced Materials (OCCAM) for assistance with materials characterization using TOF-SIMS and XPS.

■ REFERENCES

(1) Christians, J.; et al. Tailored interfaces of unencapsulated perovskite solar cells for > 1,000 h operational stability. *Nat. Energy.* **2018**, *3*, 68−74.

(2) Leijtens, T.; et al. Towards enabling stable lead halide perovskite solar cells; interplay between structural, environmental, and thermal stability. *J. Mater. Chem. A* **2017**, *5*, 11483.

(3) Rong, Y.; et al. Challenges for commercializing perovskite solar cells. *Science* **2018**, *361*, eaat8235.

(4) Duong, T.; et al. Rubidium Multication Perovskite with Optimized Bandgap for Perovskite-Silicon Tandem with over 26% Efficiency. *Adv. Energy Mater.* **2017**, *7*, 1700228.

(5) Mashhoun, S.; et al. Resolving a Critical Instability in Perovskite Solar Cells by Designing a Scalable and Printable Carbon Based Electrode-Interface Architecture. *Adv. Energy Mater.* **2018**, *8*, 1802085.

DOI: 10.1021/acsenergylett.9b00892
ACS Energy Lett. 2019, 4, 1521−1527

(6) Aristidou, N.; et al. The role of oxygen in the degradation of methylammonium lead trihalide perovskite photoactive layers. *Angew. Chem., Int. Ed.* **2015**, *54*, 8208.
(7) Pearson, A. J.; et al. Oxygen Degradation in Mesoporous Al_2O_3/$CH_3NH_3PbI_3$-xCl_x Perovskite Solar Cells: Kinetics and Mechanisms. *Adv. Energy Mater.* **2016**, *6*, 1600014.
(8) Snaith, H. J.; Hacke, P. Enabling reliability assessments of pre-commercial perovskite photovoltaics with lessons learned from industrial standards. *Nat. Energy* **2018**, *3*, 459.
(9) Leguy, A. M. A.; et al. Reversible Hydration of CH3NH3PbI3 in Films, Single Crystals, and Solar Cells. *Chem. Mater.* **2015**, *27*, 3397.
(10) Yuan, Y.; Huang, J. Ion migration in organometal trihalide perovskite and its impact on photovoltaic efficiency and stability. *Acc. Chem. Res.* **2016**, *49*, 286.
(11) Li, C.; et al. Iodine migration and its effect on hysteresis in perovskite solar cells. *Adv. Mater.* **2016**, *28*, 2446.
(12) Lee, Y. I.; et al. A Low-Temperature Thin-Film Encapsulation for Enhanced Stability of a Highly Efficient Perovskite Solar Cell. *Adv. Energy Mater.* **2018**, *8*, 1701928.
(13) Cheacharoen, R.; et al. Design and understanding of encapsulated perovskite solar cells to withstand temperature cycling. *Energy Environ. Sci.* **2018**, *11*, 144.
(14) Cheacharoen, R.; et al. Encapsulating perovskite solar cells to withstand damp heat and thermal cycling. *Sustainable Energy & Fuels* **2018**, *2*, 2398−2406.
(15) Bush, K. A.; et al. 23.6%-efficient monolithic perovskite/silicon tandem solar cells with improved stability. *Nat. Energy* **2017**, *2*, 17009.
(16) Bergmann, V. W.; et al. Local time-dependent charging in a perovskite solar cell. *ACS Appl. Mater. Interfaces* **2016**, *8*, 19402.
(17) Carrillo, J.; et al. Ionic reactivity at contacts and aging of methylammonium lead triiodide perovskite solar cells. *Adv. Energy Mater.* **2016**, *6*, 1502246.
(18) Kerner, R. A.; Rand, B. P. Ionic−Electronic Ambipolar Transport in Metal Halide Perovskites: Can. Electronic Conductivity Limit Ionic Diffusion? *J. Phys. Chem. Lett.* **2018**, *9*, 132−137.
(19) Oranskaia, A.; et al. Halogen Migration in Hybrid Perovskites: The Organic Cation Matters. *J. Phys. Chem. Lett.* **2018**, *9*, 5474−5480.
(20) Tsai, H.; et al. High-efficiency two-dimensional Ruddlesden−Popper perovskite solar cells. *Nature* **2016**, *536*, 312.
(21) Wang, Z.; et al. Efficient ambient-air-stable solar cells with 2D−3D heterostructured butylammonium-caesium-formamidinium lead halide perovskites. *Nat. Energy* **2017**, *2*, 17135.
(22) Lee, J. W.; et al. 2D perovskite stabilized phase-pure formamidinium perovskite solar cells. *Nat. Commun.* **2018**, *9*, 3021.
(23) Cho, K. T.; et al. Selective growth of layered perovskites for stable and efficient photovoltaics. *Energy Environ. Sci.* **2018**, *11*, 952−959.
(24) Kovalenko, M.; et al. Properties and potential optoelectronic applications of lead halide perovskite nanocrystals. *Science* **2017**, *358*, 745−750.
(25) Koh, T. K.; et al. Enhancing moisture tolerance in efficient hybrid 3D/2D perovskite photovoltaics. *J. Mater. Chem. A* **2018**, *6*, 2122−2128.
(26) Weidman, M. C.; et al. Highly tunable colloidal perovskite nanoplatelets through variable cation, metal, and halide composition. *ACS Nano* **2016**, *10*, 7830−7839.
(27) Quan, L. N.; et al. Ligand-stabilized reduced-dimensionality perovskites. *J. Am. Chem. Soc.* **2016**, *138*, 2649.
(28) Lin, Y.; et al. Suppressed Ion Migration in Low-Dimensional Perovskites. *ACS Energy Lett.* **2017**, *2*, 1571−1572.
(29) Grancini, G.; et al. One-Year stable perovskite solar cells by 2D/3D interface engineering. *Nat. Commun.* **2017**, *8*, 15684.
(30) Proppe, A. H.; et al. Synthetic Control over Quantum Well Width Distribution and Carrier Migration in Low-Dimensional Perovskite Photovoltaics. *J. Am. Chem. Soc.* **2018**, *140*, 2890.
(31) Bi, D.; et al. Efficient luminescent solar cells based on tailored mixed-cation perovskites. *Sci. Adv.* **2016**, *2*, No. e1501170.
(32) Yoo, J. S.; et al. Dual function of a high-contrast hydrophobic−hydrophilic coating for enhanced stability of perovskite solar cells in extremely humid environments. *Nano Res.* **2017**, *10*, 3885.
(33) Quintero-Bermudez, R.; et al. Compositional and orientational control in metal halide perovskites of reduced dimensionality. *Nat. Mater.* **2018**, *17*, 900.
(34) Mosconi, E.; et al. Light-induced annihilation of Frenkel defects in organo-lead halide perovskites. *Energy Environ. Sci.* **2016**, *9*, 3180.
(35) Matteocci, F.; et al. Interface and Composition Analysis on Perovskite Solar Cells. *ACS Appl. Mater. Interfaces* **2015**, *7*, 26176−26183.
(36) Domanski, K.; et al. Not All That Glitters Is Gold: Metal-Migration- Induced Degradation in Perovskite Solar Cells. *ACS Nano* **2016**, *10*, 6306−6314.
(37) Casaletto, M. P.; et al. XPS study of supported gold catalysts: the role of Au0 and Au+δ species as active sites. *Surf. Interface Anal.* **2006**, *38*, 215−218.
(38) Guerrero, A.; et al. Interfacial Degradation of Planar Lead Halide Perovskite Solar Cells. *ACS Nano* **2016**, *10*, 218−224.

DOI: 10.1021/acsenergylett.9b00892
ACS Energy Lett. 2019, 4, 1521−1527